The formation of amorphous alloy oxides as barriers used in magnetic tunnel junctions

J. Joshua Yang, Ying Yang, and Kaisheng Wu
Materials Science Program, University of Wisconsin–Madison, Madison, Wisconsin 53706

Y. Austin Chang[a)]
Department of Materials Science and Engineering, University of Wisconsin–Madison, Madison, Wisconsin 53706 and Materials Science Program, University of Wisconsin–Madison, Madison, Wisconsin 53706

(Received 22 February 2005; accepted 30 August 2005; published online 13 October 2005)

The quality of a tunnel barrier is of critical importance for the success of a magnetic tunnel junction. An amorphous state of the precursor metal films is beneficial for the formation of an ultrasmooth and likely defect-free oxide tunnel barrier layer, thus leading to an improved performance of a magnetic tunnel junction. However, prior to oxidation, most sputter-deposited thin films of pure metals are polycrystalline instead of amorphous. In contrast, a sputter-deposited alloy thin film could have a better amorphous-forming ability than a pure metal. Using an Al–Zr binary as an example, the amorphous-forming ability of alloy thin films was investigated thermodynamically and experimentally. A thermodynamic model was formulated to predict the compositions of a binary alloy exhibiting favorable amorphous-forming abilities when sputter-deposited alloy thin films are made. The thermodynamically calculated compositions of Al–Zr alloys with great tendencies to form amorphous metallic thin films were confirmed experimentally. The sputter-deposited alloy thin films were characterized using transmission electron microscopy and x-ray diffraction. The thermodynamic argument, applicable to any binary systems, can serve as a guide to preselect alloy compositions of any selected metallic binary with high amorphous-forming ability as precursor metals to form an oxide tunnel barrier used in a magnetic tunnel junction. © *2005 American Institute of Physics*. [DOI: 10.1063/1.2084313]

I. INTRODUCTION

Magnetic tunnel junctions (MTJs), comprised of two ferromagnetic metal electrodes (e.g., Co) separated by a thin tunnel barrier (e.g., Al_2O_3), are being widely considered for possible use as sensitive magnetic sensors and nonvolatile storage cells in magnetic random access memories (MRAM).[1–4] However, one of the major challenges is to fabricate these junctions with both high MR ratio and low product of junction resistance and area (RA) for practical applications.[5] It has been shown that the quality of the tunnel barriers plays a critical role in the success of spin-dependent tunneling in MTJs.[6,7] Considerable effort has been made to control the oxidation process of a thin Al layer in order to fabricate a high-quality tunnel barrier.[8–12] Alternative materials have also been actively studied to improve the quality of the tunnel barriers.[13–22] Among them, some alloy oxides show attractive properties to be used as MTJ tunnel barriers. The superior performance of these alloy oxide barriers is attributed to the formation of an amorphous structure in the preoxidation state in addition to a relatively low-energy band gap. As the tunnel barrier thickness is reduced in order to obtain low RA in MTJs, a rapid degradation of the MTJ properties is observed, including low TMR and high coupling fields between magnetic layers.[23] This degradation is often attributed to a lack of uniform interfaces and other defects as a result of the presence of columnar grain boundaries in the polycrystalline precursor metal films prior to oxidation.[24,25] Since a precursor metallic phase in the amorphous state has no grain boundaries,[22] it is reasonable to expect that a continuous thin layer of oxide would form when exposed to an oxidizing atmosphere, causing an improved performance of a MTJ. Indeed, Bae *et al.* reported the initial oxidizing paths of the crystalline precursors were the grain boundaries and then through the grains, leading to the formation of nonuniform interfaces and other defects[26,27] as well as the partial oxidation of the ferromagnetic layer below the tunnel barrier layer before completion of the Al oxidation.[28]

However, since an amorphous phase was found in Al–Zr alloys via different experimental techniques,[22,29–33] we choose to use this binary as a model system for both theoretical and experimental investigations in the present study. We will first present a thermodynamic formulation to predict alloy compositions of Al–Zr with tendencies to form amorphous thin films when these films are prepared using rapid quenching techniques such as sputter deposition. We will next carry out experiments to validate the thermodynamic predictions using co-sputter deposition of these alloy films. The microstructures of the alloy thin films will be characterized by transmission electron microscopy (TEM) and x-ray diffraction (XDR) as given below. When the thermodynamic

[a)]Author to whom correspondence should be addressed; electronic mail: chang@engr.wisc.edu

formulation is validated, we can then use this approach to make predictions of alloy compositions of any metallic binaries.

II. EXPERIMENT

The alloy thin films were co-deposited on rotating substrates by dc magnetron sputtering from two targets of pure Al and Zr with 6 mTorr Ar as the processing gas. The base pressure of the process chamber was less than 5×10^{-7} Torr. Different compositions of the alloy thin films were realized by varying the relative powers of the two sputter guns, which result in different sputter rates of the Al and Zr targets. The thin-film compositions were confirmed by PHI 5400 x-ray photoelectron spectroscopy (XPS) and PHI 670 Auger electron microscopy (AES). The microstructures of the thin films were characterized by Philips CM200UT transmission electron microscopy (TEM) and Panalytical X'pert x-ray diffraction (XRD). Plan view TEM samples were deposited on NaCl crystals or polymer substrates, which were then placed into water or a solvent, to let the films peel off. Thicker films were deposited on glass substrates for XRD characterization.

III. THERMODYNAMIC FORMULATION

Since fabricating thin films by sputter deposition is a rapid quenching process, as noted earlier, it is likely that the intermetallic compounds normally stable in a binary such as Al–Zr will not form under this condition due to kinetic constraints! Accordingly, we are only concerning ourselves with the relative thermodynamic stability of the (Al, Zr) amorphous phase with those of the various crystalline alloy phases. This simple model is formulated based on the bilayer structure used widely in the MTJs, but it can be used as a general model to predict the amorphous forming ability of alloy compositions in any metallic binary. A schematic diagram of a bilayer structure is given in Figs. 1(a) and 1(b), with a Co layer as the substrate and a top (Al, Zr) alloy either in the amorphous or a crystalline state. The physical dimensions of these two-layer structures are given in these figures.

The Gibbs energy of such a bilayer structure consists of three parts: the bulk Gibbs energy, the interfacial energy, and the surface energy. We will first derive the bulk Gibbs energy of such a system and then discuss the contributions from the other two parts later. The bulk Gibbs energies of the (Co)/(Al,Zr) bilayer structure, as presented in Figs. 1(a) and 1(b), are shown schematically in Fig. 1(c) as a function of the Co composition for the crystalline (Co)/crystalline (Al, Zr) and crystalline (Co)/amorphous (Al, Zr) bilayered structures, respectively. The symbols "cryst" and "am" denote the crystalline and amorphous states, respectively. As noted earlier, since we assume that the stable intermetallic compounds do not form in fabricating these films via sputter deposition due to kinetic constraints, we are only considering the (Al, Zr) solid solutions, either in a crystalline state such as the fcc in the present case denoted by "cryst," or in an amorphous state denoted by "am." Furthermore, the Gibbs energy curves of (Co) and (Al, Zr)-am or (Al, Zr)-cryst are represented by

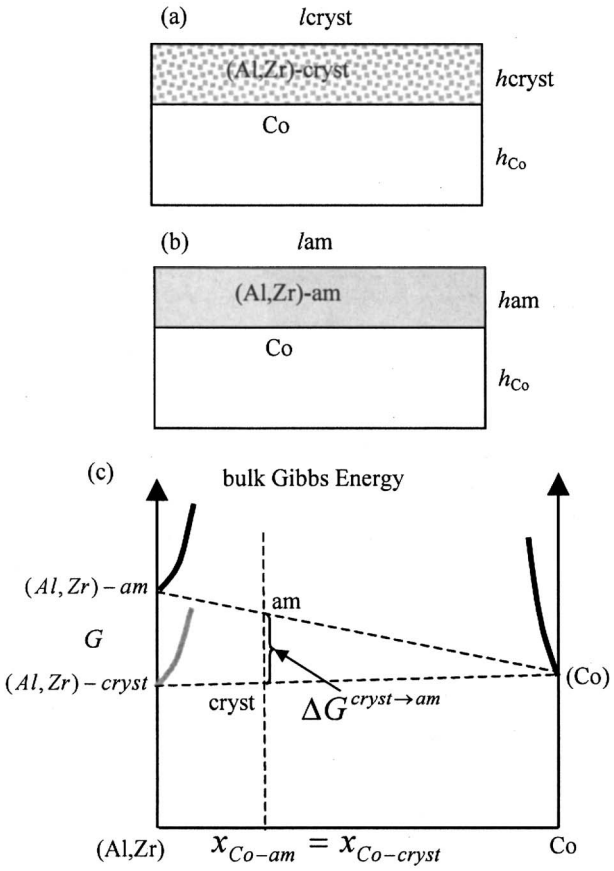

FIG. 1. Schematic diagram of the unit bilayer structures with the Al–Zr layer in (a) a crystalline state; (b) an amorphous state; (c) the bulk Gibbs energy versus the composition of Co of the bilayer in (a) and (b) for the case that (Al, Zr)-cryst is more stable than (Al, Zr)-am. l,h refers to the length and height, respectively.

sharp curves at the two ends of this figure because the mutual solubilities between Co and (Al, Zr)-am or (Al, Zr)-cryst are negligible at low temperatures ($<500\ ^\circ$C). The tangent line to the (Co) and (Al, Zr)-cryst represents the metastable phase equilibrium between Co and (Al, Zr)-cryst. Similarly, the tangent line to the (Co) and (Al, Zr)-am represents that between Co and (Al, Zr)-am. The Gibbs energy of the amorphous phase is approximated to be that of the undercooled liquid and the volume Gibbs energy of (Al, Zr)-cryst can be either lower or higher than that of amorphous phase depending on the relative stabilities of these phases. The case, assuming that (Al, Zr)-cryst is more stable, is shown in Fig. 1(c), where the overall composition in the amorphous and crystalline cases are taken to be the same, in other words, $x_{Co}^{cryst}=x_{Co}^{am}$. Thus, a vertical line can be drawn at x_{Co}^{cryst} or x_{Co}^{am} and it intersects two dashed tangent lines at two points "am" and "cryst." The energy difference defined by the vertical distance between "am" and "cryst" is represented by $\Delta G^{cryst\rightarrow am}[=\Delta G_{(Al,Zr)}^{cryst\rightarrow am}/(1-X_{Co})]$, defining the energy barrier needed to overcome in order to form the amorphous structure. The analytical equation of $\Delta G^{cryst\rightarrow am}$ at the as-deposited temperature is described by (a detailed derivation is shown in the Appendix):

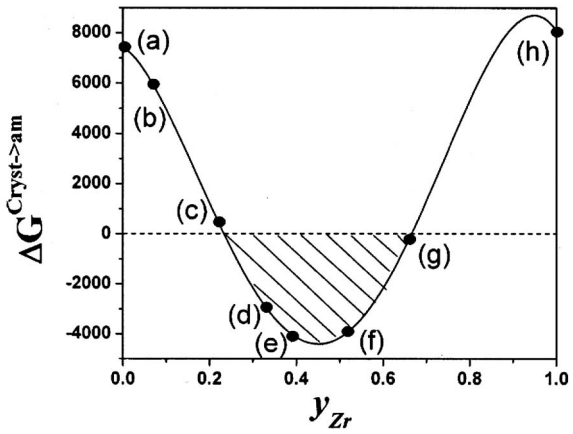

FIG. 2. The Gibbs energy difference between the fcc (Al, Zr) solution and the amorphous (Al, Zr) phases versus the composition of Zr. Co-sputter-deposited alloys were made at composition points labeled (a)–(h).

$$\frac{\Delta G^{\mathrm{cryst}\rightarrow\mathrm{am}}_{(\mathrm{Al,Zr})}}{(1-x_{\mathrm{Co}})} = y^{\mathrm{am0}}_{\mathrm{Al}}\Delta H^{\mathrm{fus}}_{\mathrm{Al}}\left(1-\frac{T_{\mathrm{as}}}{T^{\mathrm{cryst}}_{m,\mathrm{Al}}}\right) + y^{\mathrm{am0}}_{\mathrm{Zr}}\Delta H^{\mathrm{fus}}_{\mathrm{Zr}} \times\left(1-\frac{T_{\mathrm{as}}}{T^{\mathrm{cryst}}_{m,\mathrm{Zr}}}\right) + ({}^{\mathrm{ex}}G^{\mathrm{am}}_{(\mathrm{Al,Zr})} - {}^{\mathrm{ex}}G^{\mathrm{cryst}}_{(\mathrm{Al,Zr})}). \quad (1)$$

In Eq. (1), x_{Co} represents the overall composition of Co in the bilayer structure; T_{as} is the film deposition temperature; $y^{\mathrm{am}}_{\mathrm{Al}}$ and $y^{\mathrm{am}}_{\mathrm{Zr}}$ represent the composition of Al and Zr in the amorphous (Al, Zr) layer, and their summation equals unity. Since the $(1-x_{\mathrm{Co}})$ term is always positive and does not affect the sign of $\Delta G^{\mathrm{cryst}\rightarrow\mathrm{am}}$, the Co layer in the model can be replaced by other materials without changing the validity of the conclusions. The symbols $T^{\mathrm{cryst}}_{m,\mathrm{Al}}$ and $T^{\mathrm{cryst}}_{m,\mathrm{Zr}}$ refer to the transition temperatures from the pure crystalline Al and Zr to their liquid state, respectively. Similarly, ${}^{0}\Delta H^{\mathrm{fus}}_{\mathrm{Al}}$ and ${}^{0}\Delta H^{\mathrm{fus}}_{\mathrm{Zr}}$ represent the enthalpies of fusion of Al and Zr at their respective melting temperatures. The symbols ${}^{\mathrm{ex}}G^{\mathrm{am}}_{(\mathrm{Al,Zr})}$ and ${}^{\mathrm{ex}}G^{\mathrm{cryst}}_{(\mathrm{Al,Zr})}$ denote the excess Gibbs energy of the (Al, Zr) alloy in the amorphous and crystalline state. In order to evaluate the energy barrier from the (Al, Zr) crystalline to the (Al, Zr) amorphous structure, a prerequisite is to know which crystalline structure is the most stable structure. Based on the Gibbs energy of solution phases calculated from the thermodynamic description of the Al–Zr system developed by Wang *et al.*,[34] the Gibbs energy of the (Al, Zr) solution with the fcc structure is found to be the most stable crystal structure, which is consistent with the experimental results in the current study to be presented later! Therefore, the "cryst" in the aforementioned thermodynamic model can be replaced by fcc. By utilizing the lattice stability data of pure Al and Zr from SGTE (Scientific Group Thermodata Europe)[35] and the excess Gibbs energies of the undercooled liquid (Al, Zr)-am and the fcc (Al, Zr)-cryst phases calculated from the thermodynamic description developed by Wang *et al.*,[34] the value of $\Delta G^{\mathrm{cryst}\rightarrow\mathrm{am}}$ versus the composition of Zr in the top layer is plotted in Fig. 2. This plot clearly shows that the energy barrier of $\Delta G^{\mathrm{cryst}\rightarrow\mathrm{am}}$ becomes negative within a certain range of the composition of Zr, as denoted by the shaded area. The overall Gibbs energy of the bilayer is lowered when forming the amorphous state instead of the crystalline one. In other words, there is no energy barrier to form the amorphous phase!

IV. RESULTS AND DISCUSSION

Co-sputter-deposited Al–Zr alloy films with different compositions were grown to verify the thermodynamic predictions, labeled (a), (b), etc. to (h), as shown in Fig. 2. Plan view TEM micrographs and selected area diffraction (SAD) patterns of these alloy thin films are presented in Fig. 3. At the compositions (a) and (b), crystal grains and dotted SAD patterns can be clearly seen, suggesting that the Al–Zr films are polycrystalline up to 7 at. % Zr. However, at point (c) with 22 at. % Zr, most grains disappear in the micrograph and multiple diffraction rings fade with a halo ring becoming clear in the SAD patterns. This indicates a transition region from a crystalline structure to an amorphous state, which agrees with the thermodynamic calculated results that the energy barrier for an amorphous transition is close to zero at the composition of 23.5 at. % Zr. With increasing Zr concentrations the Al–Zr alloy films become a single amorphous phase, which can be seen from the single diffuse ring in SAD patterns and typical amorphous micrographs[36] (defocused to enhance the contrast) at the composition points (d), (e), (f), and (g), consistent with values predicted by the thermodynamic calculations. At point (h), the Zr composition reaches 100 at. % and a polycrystalline fcc structure can be clearly observed from the micrograph and SAD pattern. This suggests another transition region located in between points (g) and (h), where the films transform from an amorphous state back to a crystalline structure again. Thicker films with typical compositions were deposited on glass for the XRD structure characterization, as shown in Fig. 4. In the three XRD diffraction patterns, the big humps at about 24° result from the glass substrate, which was adopted to exclude any possible peaks from the substrate. The crystal diffraction peaks of Zr and Al can be clearly seen in the 260 nm pure Zr and Al films, respectively, while no diffraction peak can be observed in the 300 nm $Al_{0.67}Zr_{0.33}$ alloy film, which is consistent with the TEM observation.

In view of the simplicity of the thermodynamic formation, it is indeed surprising that there is such a good agreement between the calculation and the experimentation in terms of the alloy compositions for an amorphous formation ability. It is worth noting that Yoshioka *et al.* reported larger alloy compositions, i.e., 17–71 at. % Zr, for amorphous phase formation in this binary.[32] Since they made their films by sputter deposition from an Al target with Zr chips instead of co-sputtering, it is likely that the XRD structure characterization method is not sufficiently sensitive to characterize the presence of a small amount of crystalline materials in the alloy films. On the other hand, the TEM is a more suitable tool for structure characterization in this case.

The reason why the amorphous phase is more stable than the crystalline phase will be addressed below. According to Eq. (1), two factors contribute to the relative stability of these two phases, i.e., the fusion enthalpies of pure Al and pure Zr and the relative excess Gibbs energies of the amorphous phase versus that of the crystalline phases. Since the

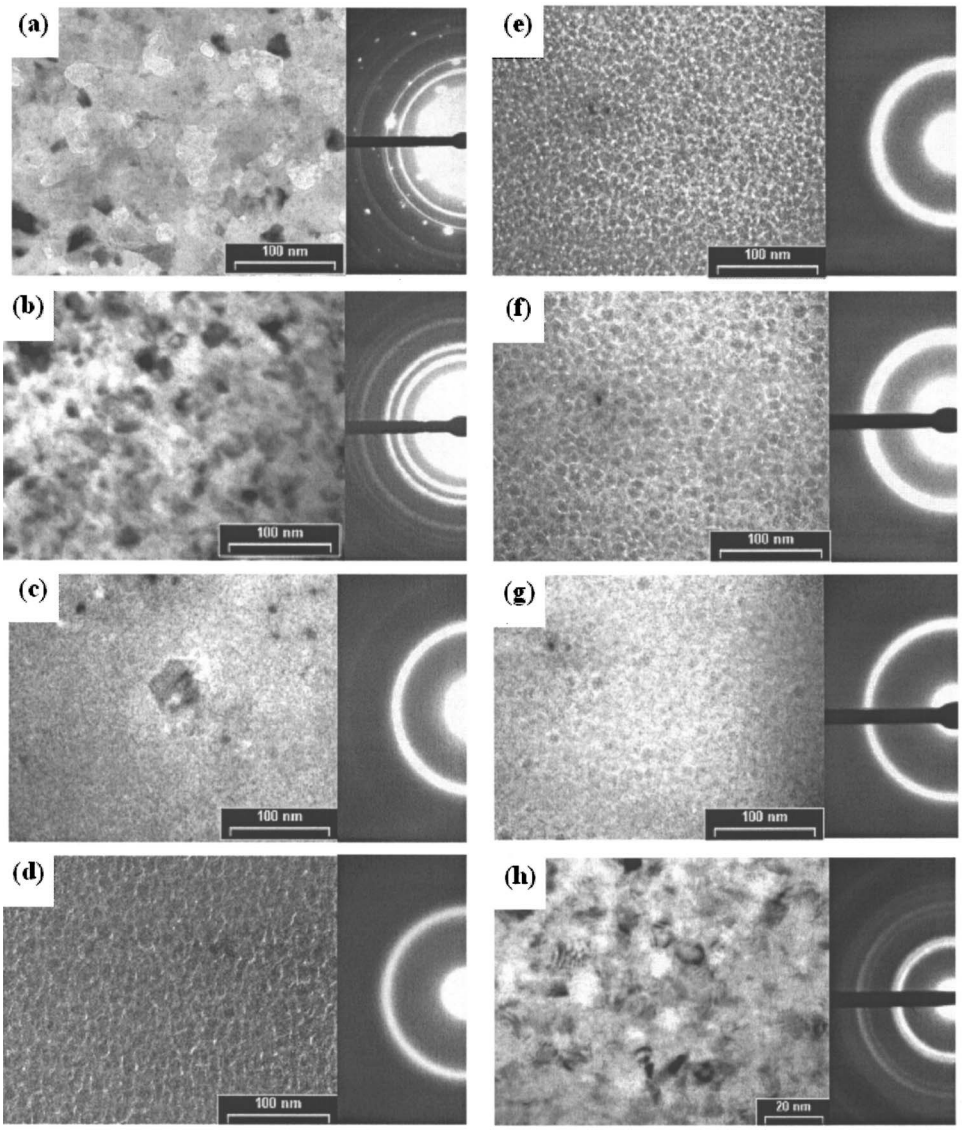

FIG. 3. TEM micrographs and SAD patterns of Co-sputter-deposited Al–Zr alloy films with compositions of (a) 0 at. %, (b) 7 at. %, (c) 22 at. %, (d) 33 at. %, (e) 39 at. %, (f) 52 at. %, (g) 66 at. %, and (h) 100 at. % Zr.

fusion enthalpies of pure Al and Zr are positive, the negative value of $\Delta G_{(\mathrm{Al,Zr})}^{\mathrm{cryst}\rightarrow\mathrm{am}}$ requires that the excess energy of the crystalline phase must be more positive than that of the amorphous phase. From a thermodynamic point of view, the excess energy consists of two parts, i.e., chemical interaction and elastic energy. The chemical interaction in the amorphous structure is expected to be comparable with that of the disordered solid solution since both structures are chemically disordered. Therefore, the important source to increase the excess energy of the fcc phase is due to an increase in the elastic strain energy induced by lattice mismatch, i.e., large size differences between the two component elements. When the elastic strain energy reaches a critical level, it will lead to a topological instability of the crystalline lattice. The amorphous phase will not accumulate too much elastic strain energy due to its inherently more flexible bonds and long-range topological disorder. The atomic radii of Al and Zr are 0.182 nm and 0.216 nm, respectively. The size mismatch of 18.8% between them is significant enough to produce large strain energy.

It should be pointed out that the Gibbs energy contribution from the surface and interfacial energies in the thin film with nanoscale thickness should not be ignored. However, it has been reported in the literature[37] that the surface and interfacial energies involving amorphous phases are generally lower than those of the crystalline counterparts, and thus

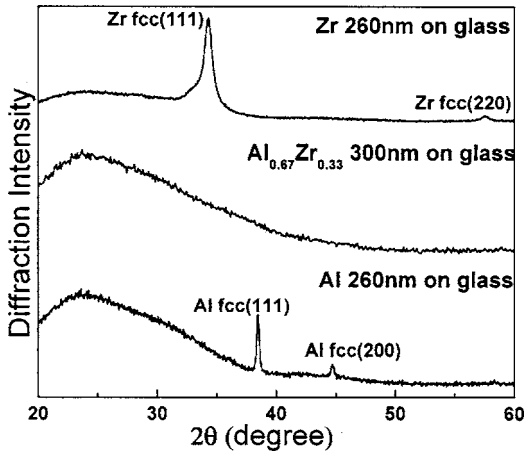

FIG. 4. The XRD results of three typical films on glass: pure Zr 260 nm, $Al_{0.67}Zr_{0.33}$ 300 nm and pure Al 260 nm.

these energies actually favor the formation of an amorphous phase. Therefore, the surface energy and interfacial energy will not violate the conclusion drawn from the bulk Gibbs energy calculation.

The thermodynamic characteristic of the Al–Zr system gives a clue to the formation of the amorphous phase and enables us to select other binary systems and compositions for oxide tunnel barrier applications. Based on the above thermodynamic argument for the Al–Zr model system and available thermodynamic data as well as the low band gap consideration of the metal oxides, the metallic elements of Al, Mg, Ti, Nb, Ta, Hf, Zr, Y, and some rare earth metals could be alloyed with each other for the use of precursor metals of an oxide tunnel barrier in MTJs.

V. CONCLUSIONS

Within a composition range of 23.5–67.5 at. % Zr in the Al–Zr binary system, the amorphous phase has been found thermodynamically more stable than the crystalline phase in Co-sputter-deposited Al–Zr alloy thin films. The thermodynamic analysis for the Al–Zr alloys is consistent with experimentally obtained results. On the basis of this study for an Al–Zr binary, it is reasonable to conclude that this analysis can be used as a guide to preselect alloy compositions of any binary system with great amorphous forming ability, and thus could produce a high-quality oxide tunnel barrier in a MTJ.

ACKNOWLEDGMENTS

This work is supported by a grant from the Division of Materials Science, Office of Basic Energy Research of Department of Energy under Grant No. DE-FG02-99ER45777 and the Wisconsin Distinguished Professorship.

APPENDIX

At the as-deposited temperature Co–(Al, Zr),

$$G^{\text{cryst}}_{(\text{Al,Zr})} = x^{\text{cryst}}_{(\text{Al,Zr})}\,{}^{0}G^{\text{cryst}}_{(\text{Al,Zr})} + x_{\text{Co}}\,{}^{0}G^{\text{cryst}}_{\text{Co}}$$
$$= x^{\text{cryst}}_{(\text{Al,Zr})}\left\{ y^{\text{cryst}0}_{\text{Al}}G^{\text{cryst}}_{\text{Al}} + y^{\text{cryst}0}_{\text{Zr}}G^{\text{cryst}}_{\text{Zr}} + RT\begin{bmatrix} y^{\text{cryst}}_{\text{Al}}\ln y^{\text{cryst}}_{\text{Al}} \\ y^{\text{cryst}}_{\text{Zr}}\ln y^{\text{cryst}}_{\text{Zr}} \end{bmatrix} + {}^{\text{ex}}G^{\text{cryst}}_{(\text{Al,Zr})} \right\} + x_{\text{Co}}\,{}^{0}G^{\text{cryst}}_{\text{Co}},$$

$$G^{\text{am}}_{(\text{Al,Zr})} = x^{\text{am}}_{(\text{Al,Zr})}\,{}^{0}G^{\text{am}}_{(\text{Al,Zr})} + x_{\text{Co}}\,{}^{0}G^{\text{cryst}}_{\text{Co}}$$
$$= x^{\text{am}}_{(\text{Al,Zr})}\left\{ y^{\text{am}0}_{\text{Al}}G^{\text{am}}_{\text{Al}} + y^{\text{am}0}_{\text{Zr}}G^{\text{am}}_{\text{Zr}} + RT\begin{bmatrix} y^{\text{am}}_{\text{Al}}\ln y^{\text{am}}_{\text{Al}} \\ +\, y^{\text{am}}_{\text{Zr}}\ln y^{\text{am}}_{\text{Zr}} \end{bmatrix} + {}^{0}G^{\text{am}}_{(\text{Al,Zr})} \right\} + x_{\text{Co}}\,{}^{0}G^{\text{cryst}}_{\text{Co}},$$

$$\Delta G^{\text{cryst}\rightarrow\text{am}}_{(\text{Al,Zr})} = x^{\text{am}}_{(\text{Al,Zr})}y^{\text{am}}_{\text{Al}}({}^{0}G^{\text{am}}_{\text{Al}} - {}^{0}G^{\text{cryst}}_{\text{Al}}) + x^{\text{am}}_{(\text{Al,Zr})}y^{\text{am}}_{\text{Zr}}({}^{0}G^{\text{am}}_{\text{Zr}} - {}^{0}G^{\text{cryst}}_{\text{Zr}}) + x^{\text{am}}_{(\text{Al,Zr})}({}^{\text{ex}}G^{\text{am}}_{(\text{Al,Zr})} - {}^{\text{ex}}G^{\text{cryst}}_{(\text{Al,Zr})}).$$

Since

$$x_{(\text{Al,Zr}-a)} = 1 - x_{\text{Co}},$$

$$\Delta G^{\text{cryst}\rightarrow\text{am}}_{\text{Al,Zr}} = (1 - x_{\text{Co}})\left[y^{\text{am}0}_{\text{Al}}\Delta H^{\text{fus}}_{\text{Al}}\left(1 - \frac{T_{as}}{T_{m,\text{Al}}}\right) + y^{\text{am}0}_{\text{Zr}}\Delta H^{\text{fus}}_{\text{Zr}}\left(1 - \frac{T_{as}}{T_{m,\text{Zr}}}\right) + {}^{\text{ex}}G^{\text{am}}_{(\text{Al,Zr})} - {}^{\text{ex}}G^{\text{cryst}}_{(\text{Al,Zr})}\right].$$

[1] S. A. Wolf, D. D. Awschalom, R. A. Buhrman, J. M. Daughton, S. von Molnár, M. L. Roukes, A. Y. Chtchelkanova, and D. M. Treger, Science **294**, 1488 (2001).
[2] J. S. Moodera, L. R. Kinder, T. M. Wong, and R. Meservey, Phys. Rev. Lett. **74**, 3273 (1995).
[3] I. Zutic, J. Fabian, and S. D. Sarma, Rev. Mod. Phys. **76**, 323 (2004).
[4] G. A. Prinz, Science **282**, 1660 (1998).
[5] H. Shim, B. K. Cho, J. Kim, T. W. Kim, and W. J. Park, J. Appl. Phys. **93**, 7026 (2003).
[6] J. S. Moodera, J. Nassar, and G. Mathon, Annu. Rev. Mater. Sci. **29**, 381 (1999).
[7] E. Y. Tsymbal, O. N. Mryasov, and P. R. LeClair, J. Phys.: Condens. Matter **15**, R109 (2003).
[8] K. Ohashi, K. Hayashi, K. Nagahara, K. Ishihara, E. Fukami, J. Fujikata, S. Mori, M. Nakada, T. Mitsuzuka, K. Matsuda, H. Mori, A. Kamijo, and H. Tsuge, IEEE Trans. Magn. **36**, 2549 (2000).
[9] J. J. Sun, K. Shimazawa, N. Kasahara, K. Sato, T. Kagami, S. Saruki, S. Araki, and M. Matsuzaki, J. Appl. Phys. **89**, 6653 (2001).
[10] Z. G. Zhang, P. P. Freitas, A. R. Ramos, N. P. Barradas, and J. C. Soares, Appl. Phys. Lett. **79**, 2219 (2001).
[11] J. R. Childress, M. M. Schwickert, R. E. Fontana, M. K. Ho, P. M. Rice, and B. A. Gurney, J. Appl. Phys. **89**, 7353 (2001).
[12] J. J. Yang, P. F. Ladwig, Y. Yang, C.-X. Ji, F. X. Liu, B. B. Pant, A. E. Schultz, and Y. A. Chang, J. Appl. Phys. **97**, 10C918-1 (2005).
[13] Z. Li, C. d. Groot, and J. H. Moodera, Appl. Phys. Lett. **77**, 3630 (2000).
[14] P. Rottländer, M. Hehn, O. Lenoble, and A. Schuhl, Appl. Phys. Lett. **78**, 3274 (2001).
[15] J. Wang, P. P. Freitas, E. Snoeck, P. Wei, and J. C. Soares, Appl. Phys. Lett. **79**, 4387 (2001).
[16] S. S. P. Parkin, United States Patent 6,359,289.
[17] X. Jiang, Alex F. Panchula, and S. S. P. Parkin, Appl. Phys. Lett. **83**, 5244 (2003).
[18] J. Faure-Vincent, C. Tiusan, E. Jouguelet, F. Canet, M. Sajieddine, C. Bellouard, E. Popova, M. Hehn, F. Montaigne, and A. Schuhl, Appl. Phys. Lett. **82**, 4507 (2003).
[19] M. Bibes, M. Bowen, A. Barthélémy, A. Anane, K. Bouzehouane, C. Carrétéro, E. Jacquet, J.-P. Contour, and O. Durand, Appl. Phys. Lett. **82**, 3269 (2003).
[20] B. G. Park, T. D. Lee, T. H. Lee, C. G. Kim, and C. O. Kim, J. Appl. Phys. **93**, 6423 (2003).
[21] M. Bowen, M. Bibes, A. Barthélémy, J.-P. Contour, A. Anane, Y. Lemaître, and A. Fert, Appl. Phys. Lett. **82**, 233 (2003).
[22] S. Lee, C. Choi, and Y. Kim, Appl. Phys. Lett. **83**, 317 (2003).
[23] H. Boeve, J. De Boeck, and G. Borghs, J. Appl. Phys. **89**, 482 (2001).
[24] D. Allen, R. Schad, G. Zangari, I. Zana, D. Yang, M. Tondra, and D. Wang, J. Appl. Phys. **87**, 5188 (2000).
[25] U. Rüdiger, R. Calarco, U. May, K. Samm, J. Hauch, H. Kittur, M. Sperlich, and G. Güntherodt, J. Appl. Phys. **89**, 7573 (2001).
[26] J. S. Bae, K. H. Shin, T. D. Lee, and H. M. Lee, Appl. Phys. Lett. **80**, 1168 (2002).
[27] Y. Ando, M. Hayashi, S. Iura, K. Yaoita, C. C. Yu, H. Kubota, and T. Miyazaki, J. Phys. D **35**, 2415 (2002).
[28] A. E. T. Kuiper, M. F. Gillies, V. Kottler, G. W. 't Hooft, J. G. M. van Berkum, C. van der Marel, Y. Tamminga, and J. H. M. Snijders, J. Appl. Phys. **89**, 1965 (2001).
[29] E. Ma and M. Atzmon, Phys. Rev. Lett. **67**, 1126 (1991).
[30] E. Ma, F. Brunner, and M. Atzmon, J. Phase Equilib. **14**, 137 (1993).

[31]H. J. Fecht, G. Han, Z. Fu, and W. L. Johnson, J. Appl. Phys. **67**, 1744 (1990).
[32]H. Yoshioka, H. Habazaki, A. Kawashima, K. Asami, and K. Hashimoto, Electrochim. Acta **36**, 1227 (1991).
[33]J. Ho and K. Lin, J. Appl. Phys. **75**, 2434 (1994).
[34]T. Wang, Z. Jin, and J. Zhao, J. Phase Equilib. **22**, 544 (2001).
[35]A. T. Dinsdale, CALPHAD: Comput. Coupling Phase Diagrams Thermochem. **15**, 317 (1991).
[36]D. B. Williams and C. B. Carter, *Transmission Electron Microscopy: A Textbook For Materials Science* (Plenum, New York, 1996), Chap. 28.
[37]R. Benedictus, R. Bottger, and E. J. Mittemeijer, Phys. Rev. B **54**, 9109 (1996).